Driver mutations of the adenoma-carcinoma sequence govern the intestinal epithelial global translational capacity

Wouter Laurentius Smit[a], Claudia Nanette Spaan[a], Ruben Johannes de Boer[a], Prashanthi Ramesh[b,c], Tânia Martins Garcia[a], Bartolomeus Joannes Meijer[a], Jacqueline Ludovicus Maria Vermeulen[a], Marco Lezzerini[d], Alyson Winfried MacInnes[d], Jan Koster[e], Jan Paul Medema[b,c], Gijs Robert van den Brink[a,f], Vanesa Muncan[a], and Jarom Heijmans[a,g,1]

[a]Department of Gastroenterology and Hepatology, Tytgat Institute for Liver and Intestinal Research, Amsterdam University Medical Center, University of Amsterdam, 1105 BK Amsterdam, The Netherlands; [b]Laboratory for Experimental Oncology and Radiobiology, Center for Experimental and Molecular Medicine, Cancer Center Amsterdam, Amsterdam University Medical Center, University of Amsterdam, 1105 AZ Amsterdam, The Netherlands; [c]Oncode Institute, Amsterdam UMC, University of Amsterdam, 1105 AZ Amsterdam, The Netherlands; [d]Laboratory for Genetic Metabolic Diseases, Amsterdam University Medical Center, University of Amsterdam, 1105 AZ Amsterdam, The Netherlands; [e]Department of Oncogenomics, Amsterdam University Medical Center, University of Amsterdam, 1105 AZ Amsterdam, The Netherlands; [f]Roche Innovation Center Basel, F. Hoffmann-La Roche AG, 4070 Basel, Switzerland; and [g]Department of Internal Medicine and Hematology, Amsterdam University Medical Center, University of Amsterdam, 1105 AZ Amsterdam, The Netherlands

Edited by Napoleone Ferrara, University of California San Diego, La Jolla, CA, and approved August 26, 2020 (received for review July 25, 2019)

Deregulated global *mRNA* translation is an emerging feature of cancer cells. Oncogenic transformation in colorectal cancer (CRC) is driven by mutations in *APC*, *KRAS*, *SMAD4*, and *TP53*, known as the adenoma-carcinoma sequence (ACS). Here we introduce each of these driver mutations into intestinal organoids to show that they are modulators of global translational capacity in intestinal epithelial cells. Increased global translation resulting from loss of *Apc* expression was potentiated by the presence of oncogenic $Kras^{G12D}$. Knockdown of *Smad4* further enhanced global translation efficiency and was associated with a lower 4E-BP1-to-eIF4E ratio. Quadruple mutant cells with additional P53 loss displayed the highest global translational capacity, paralleled by high proliferation and growth rates, indicating that the proteome is heavily geared toward cell division. Transcriptional reprogramming facilitating global translation included elevated ribogenesis and activation of mTORC1 signaling. Accordingly, interfering with the mTORC1/4E-BP/eIF4E axis inhibited the growth potential endowed by accumulation of multiple drivers. In conclusion, the ACS is characterized by a strongly altered global translational landscape in epithelial cells, exposing a therapeutic potential for direct targeting of the translational apparatus.

global translation | protein synthesis | colorectal cancer | driver mutations

The adenoma-carcinoma sequence (ACS) is defined by a set of recurrent driver mutations in *APC*, *KRAS*, *SMAD4*, and *TP53* genes, that accumulate during adenoma formation and progression to sporadic colorectal cancer (CRC), often correlating with specific stages of the developmental process (1). Since its early description by Vogelstein and colleagues, a body of research has further supported and elaborated on this well-established paradigm (2), and the putative oncogenic potential of each mutation has been demonstrated in various genetic rodent models (3). It is well known that driver mutations deregulate specific cell signaling pathways, but how this ultimately leads to oncogenic transformation of a healthy intestinal cell remains to be understood. Over the past decade, mounting evidence has indicated that quantitative and qualitative alterations in *mRNA* translation are a prominent feature of various cancers (4). Global *mRNA* translation can be defined as the capacity of the cell's translation apparatus to produce nascent polypeptides in order to maintain the cellular proteome. The translational apparatus consists of the *mRNA* transcripts, ribosomes, translation factors, and aminoacyl-*tRNAs*. Cancer cells exploit the translational apparatus by deregulating these components, which is supported by multiple lines of evidence, including altered expression translation factors (4), ribosomal proteins and ribosomal *RNA* (*rRNA*) (5), and the presence of oncogenes such as PIK3CA and c-MYC, that modulate translational control (6). Thus, through aberrant signaling of pathways that converge on the translational apparatus, specific oncogenes may utilize entire proteomic programs in order to drive oncogenic transformation of a normal cell (7).

In the majority of sporadic CRCs, accumulation of a few driver mutations is considered to be sufficient in coordinating many of the cell-intrinsic aspects of oncogenic transformation, which epithelial cancer cells must adopt to clonally expand, invade, and metastasize (8). Although the transcriptomic layers underpinning this complex process have been studied extensively, effects on specific translational programs, as well as the global translational capacity itself, are largely unknown. Recently, it has been shown that *Apc*-deficient mouse intestinal cells harbor increased global translation rates via mTORC1-mediated modulation of translation elongation (9). This study clearly demonstrated that interfering with global translation through the mTORC1/S6K/eEF2K axis strongly impaired intestinal epithelial hyperproliferation and tumorigenesis caused by deficiency of *Apc*. Moreover, we have

Significance

Deregulated global *mRNA* translation is a feature of various cancers and considered important in oncogenic transformation. In colorectal cancer (CRC), the role of the most common driver mutations in *APC*, *KRAS*, *SMAD4*, and *TP53* on the global translational capacity are incompletely understood. Here, using mouse and human intestinal organoids, we found that each mutation governs the global translational capacity of the epithelial cell. Global translation is linked to known oncogenic hallmarks, including cell proliferation and growth upon accumulation of these mutations, posing the translational apparatus as a potential therapeutic target in CRC.

Author contributions: W.L.S., A.W.M., G.R.v.d.B., V.M., and J.H. designed research; W.L.S., C.N.S., R.J.d.B., P.R., T.M.G., B.J.M., J.L.M.V., and M.L. performed research; J.K. and J.P.M. contributed new reagents/analytic tools; W.L.S. and C.N.S. analyzed data; and W.L.S. wrote the paper.

The authors declare no competing interest.

This article is a PNAS Direct Submission.

[1]To whom correspondence may be addressed. Email: j.heijmans@amsterdamumc.nl.

This article contains supporting information online at https://www.pnas.org/lookup/suppl/doi:10.1073/pnas.1912772117/-/DCSupplemental.

First published September 28, 2020.

recently shown that heterozygous expression of chaperone GRP78, which leads to repression of p-eIF2α-mediated global translation, reduced adenoma formation in *Apc*-deficient mice (10). Interestingly, these studies have shown that genetically interfering with global translation predominantly affected *Apc*-deficient epithelium, with no obvious discernible phenotype of the epithelium during homeostasis (9, 10). This suggests that epithelial cells that exhibit functional loss of APC rely on ample global translational output during adenoma formation, displaying the importance of translational efficiency in transformed cells. Furthermore, efficient *mRNA* translation, which mainly determines the mammalian cellular proteome (11), may be particularly important for maintaining the oncogenic proteome in a cancer cell that must overcome repressed global translation when exposed to cellular stress (12).

It remains to be investigated whether the main driver mutations associated with CRC development affect the global translational capacity of the intestinal epithelial cell. To address this, we studied the impact of oncogenic mutations in *APC*, *KRAS*, *SMAD*, and *TP53* on the global translational capacity of primary intestinal epithelial cells. Our data reveal a highly altered global translational landscape throughout the ACS, in which multiple driver mutations contribute to further enhance the global translational capacity.

Results

Mutations in *Apc* and *Kras* Drive Epithelial Stemness and Enhance the Rate of Global Translation, Proliferation, and Ribogenesis. To study the effect of specific driver mutations on the global translational capacity, we made use of small intestinal organoids to model the ACS. First, we assessed loss of APC function, a strongly predisposing event that occurs in early transformation of intestinal epithelium in almost 80% of CRC cases (13). Organoids that were derived from inducible *Villin-CreER^{T2}-Apc$^{580S/580S}$* mice were recombined in vitro with 4OH-tamoxifen. As expected, these organoids adopted a cystic morphology and grew in the absence of WNT agonist R-spondin (*SI Appendix*, Fig. S1 *A*, *Left*). Stem cells were enriched at the cost of differentiated cell types, as indicated by transcriptional up-regulation of crypt base columnar stem cell markers *Lgr5*, *Ascl2*, *Olfm4*, *Cd44*, and *Sox9*, together with down-regulation of the lineage-specific differentiation markers *Lyz1*, *Muc2*, *Chga*, and *Alpi* (Fig. 1 *A* and *B*). Expansion of the proliferative stem cell compartment following *Apc* loss has been well described and results from constitutive autonomous Wnt/β-catenin signaling that promotes stemness and prevents normal differentiation (14). Using L-[^{35}S]-methionine incorporation, we compared the rate of global translation between *Apc$^{-/-}$* cells in organoids recombined for several weeks to their nonrecombined *Apc$^{fl/fl}$* counterparts, and observed a striking increase, consistent with recently published findings (*SI Appendix*, Fig. S1*B*) (9). To validate the methodology, in which quantification of global translation was normalized to the proteomic biomass, we used flow cytometry-based L-azidohomoalanine (AHA) incorporation in order to measure global translation rates per individual cell. Similarly, AHA incorporation rates in *Apc$^{-/-}$* organoids were strongly increased (*SI Appendix*, Fig. S1*C*). To assess whether altered translation is a direct consequence of the introduced mutation, or whether it follows secondary events emanating from the transformation by deletion of *Apc*, we measured global translation directly after recombination. Already at 48 h, when *Cre*-mediated gene-to-protein turnover has just been established (15), there was a 26% increase in the global translation rate (*SI Appendix*, Fig. S1*D*). This is in line with recent findings in which *Apc* deletion was achieved by recombination in vivo, and a similar impact on global translation was observed in organoid cultures assessed directly ex vivo (9). We also found the translation rate to increase over time after deletion of *Apc*, comparing 48-h recombination to several weeks (*SI Appendix*, Fig. S1 *B* and *D*). To assess if reduced epithelial WNT signaling affected global translation in wild-type cells, we withdrew canonical WNT agonist R-spondin for 24 h from the culture medium of wild-type organoids. As expected, when WNT signaling could not be sustained, the rate of global translation declined (*SI Appendix*, Fig. S1*E*).

Clinically, human loss-of-function mutations in the *APC* gene usually precede or coincide with gain-of-function mutations in the oncogene *KRAS*, as illustrated by *KRAS* point mutations present in 40 to 50% of CRCs at early stages (16). The most frequent mutation is a base substitution *KRAS^{G12D}*, a conversion of glycine (G) to aspartic acid (D), that renders RAS in an active GTP-bound state causing continuous activation of RAS signaling (17). To model this event, we studied whether *Kras^{G12D}* modulated global translation in wild-type and *Apc*-deleted epithelium. Using inducible heterozygous organoids from *Villin-CreER^{T2}-Kras$^{+/G12D}$* transgenic mice, we generated organoids that grew independent of culture factor EGF after in vitro recombination (*SI Appendix*, Fig. S1 *A*, *Middle*). *Kras$^{+/G12D}$* organoids exhibited an enlarged central lumen with maintained pericentral budding, a phenotype that differed from both *Apc$^{-/-}$* and wild-type organoids (*SI Appendix*, Fig. S1 *A*, *Middle*). Interestingly, further characterization revealed significant reduction of WNT-related stemness marker genes (Fig. 1*C*). Differentiation appeared skewed toward a goblet cell phenotype with loss of other secretory cell types, as indicated by higher *Muc2* expression in parallel with very low expression of *Lyz1* and *Chga* (Fig. 1*D*). This was confirmed by immunohistochemistry (IHC) which showed increased numbers of periodic acid–Schiff (PAS)- and MUC2-positive cells in *Kras$^{+/G12D}$* organoids (*SI Appendix*, Fig. S1*F*). Consistent with altered stem cell fate, NOTCH target gene *Hes1*, a fate regulator that suppresses precocious differentiation to the secretory lineage, was decreased (*SI Appendix*, Fig. S1*G*) (18). Importantly, these findings are consistent with increased goblet cell formation seen in transgenic *Kras^{G12D}* mice, underscoring the similarities with ex vivo organoid models when studying epithelial mutations (19). Subsequently, we analyzed organoids where *Apc* was deleted in the presence of *Kras^{G12D}*, using *Apc$^{fl/fl}$Kras$^{+/fl}$* organoids that were recombined in vitro (*Apc$^{-/-}$Kras$^{+/G12D}$*) (*SI Appendix*, Fig. S1 *A*, *Right*). Although stemness was markedly reduced in the *Kras$^{+/G12D}$* organoids, *Apc$^{-/-}$Kras$^{+/G12D}$* organoids harbored clear stem cell enrichment with barely detectable differentiation markers (Fig. 1 *E* and *F*). Next, we studied how *Kras^{G12D}* affected the global translational capacity in the presence and absence of deleted *Apc*. Interestingly, *Kras^{G12D}* only enhanced the global translation rate in combination with loss of *Apc* (Fig. 1*G*). To show that epithelial RAS signaling controls global translation, we withdrew culture factor EGF, a direct activator of RAS, which led to a reduction of the global translational capacity in wild-type cells (*SI Appendix*, Fig. S1*H*). Thus, *Kras^{G12D}*-mediated activation of RAS signaling further enhances the global translational capacity of *Apc*-deleted intestinal epithelial cells.

mRNA translation is a cell biological process that is intimately linked to proliferation under both homeostatic conditions and in cancer (20), although these processes can be uncoupled (21). To correlate global translation to proliferation rates, we assessed incorporation of 5-bromo-2-deoxyuridine (BrdU) normalized to the number of DAPI→positive cells per organoid, in order to quantify the percentage of proliferating cells of *Kras$^{+/G12D}$*, *Apc$^{-/-}$*, and *Apc$^{-/-}$Kras$^{+/G12D}$* organoids. Changes in proliferation paralleled the rate of global translation, implying that these properties are linked, even under these hyperproliferative conditions (Fig. 1*H*). Continuous, elevated levels of protein synthesis are needed to fuel proliferation, requiring coordinated production of components of the translational apparatus, including cytoplasmic ribosomal proteins and ribosomal *RNAs* (22). Using microarray analysis, we searched for transcriptional reprogramming that could facilitate the increased global translation observed

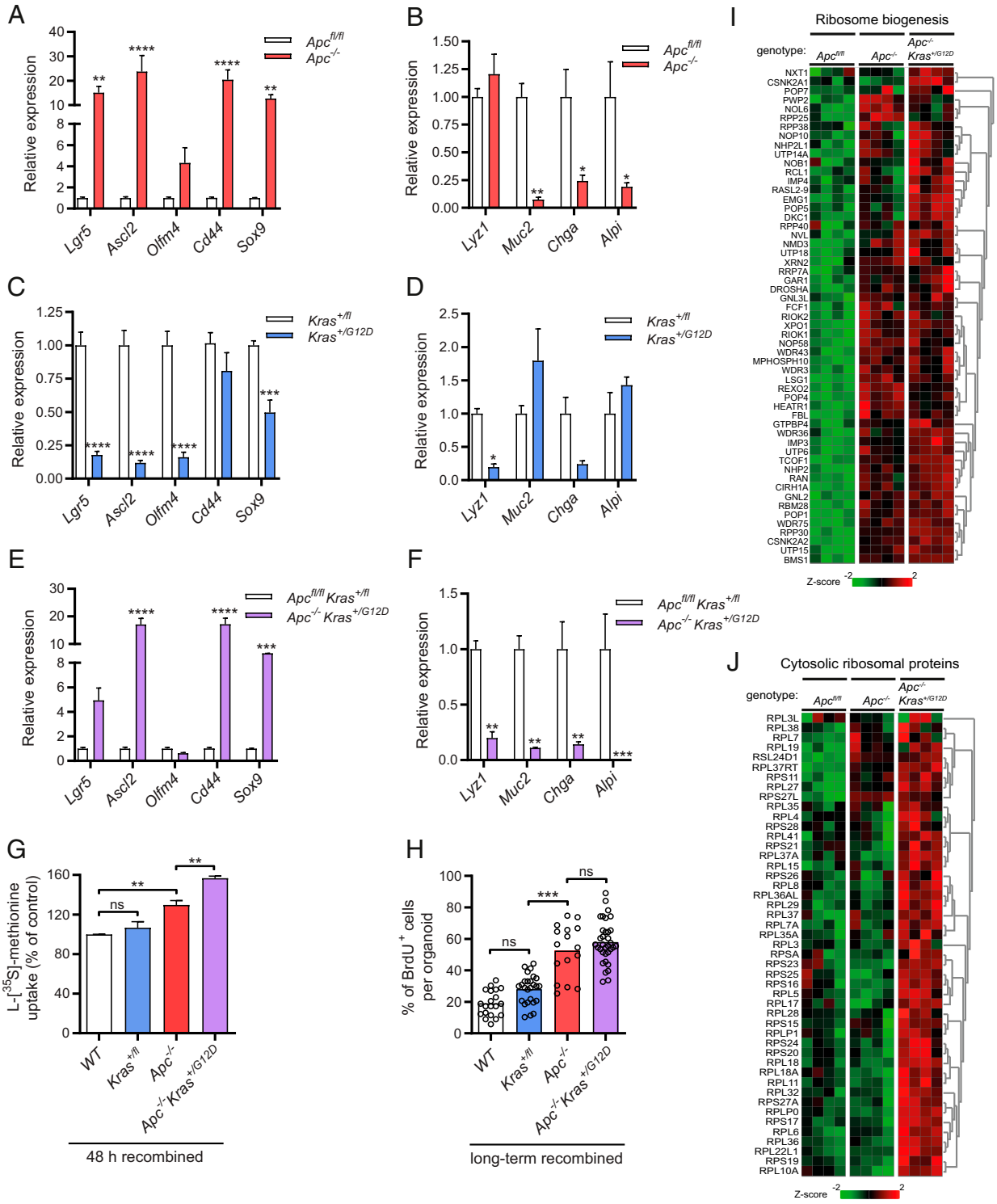

Fig. 1. Loss of Aps and additional transgenic expression of oncogenic $Kras^{G12D}$ organoids leads to stem cell enrichment, increased rates of global translation, proliferation, and ribogenesis. (*A*) Quantitative RT-PCR analysis of crypt base columnar stem cell markers in long-term (>2 wk) recombined $Apc^{-/-}$ organoids ($n = 3$). (*B*) Analysis of differentiation markers in long-term recombined (>2 wk) $Apc^{-/-}$ organoids ($n = 3$). (*C*) Quantitative RT-PCR analysis of crypt base columnar stem cell markers in long-term (>2 wk) recombined $Kras^{+/G12D}$ organoids ($n = 3$). (*D*) Quantitative RT-PCR analysis of differentiation markers in long-term (>2 wk) recombined $Kras^{+/G12D}$ organoids ($n = 3$). (*E*) Quantitative RT-PCR analysis of crypt base columnar stem cell markers in long-term (>2 wk) recombined $Apc^{-/-}Kras^{+/G12D}$ organoids ($n = 3$). (*F*) Quantitative RT-PCR analysis of differentiation markers in long-term (>2 wk) recombined $Apc^{-/-}Kras^{+/G12D}$ organoids ($n = 3$). (*G*) L-[^{35}S]-methionine incorporation assay in $Kras^{+/G12D}$, $Apc^{-/-}$, and $Apc^{-/-}Kras^{+/G12D}$ organoids, 48 h after recombination. (*H*) Quantification of BrdU immunostaining, showing the percentage of BrdU-positive cells per organoid in long-term (>2 wk) recombined $Kras^{+/G12D}$, $Apc^{-/-}$, and $Apc^{-/-}Kras^{+/G12D}$ organoids. (*I*) Heatmap of microarray *mRNA* expression data containing genes related to *rRNA* production, processing, and ribosome assembly in $Apc^{-/-}$ and $Apc^{-/-}Kras^{+/G12D}$ organoids ($n = 4$). (*J*) Heatmap of microarray *mRNA* expression data containing genes encoding for cytosolic ribosomal protein in wild-type, $Apc^{-/-}$, and $Apc^{-/-}Kras^{+/G12D}$ organoids ($n = 4$). Data are represented as means ± SEM. Significance (one-way ANOVA) $*P < 0.05$, $**P < 0.01$, $***P < 0.001$, $****P < 0.0001$.

in $Apc^{-/-}$ and $Apc^{-/-}Kras^{+/G12D}$ cells. Gene ontology analysis revealed that genes associated with *rRNA* production, processing and ribosome assembly were strongly up-regulated, particularly at the step of *Apc* loss (Fig. 1*I*). Furthermore, additional $Kras^{G12D}$ led to up-regulation of a majority of all genes encoding for cytoplasmic large and small ribosomal proteins (RPLs and RPSs), the protein constituents of the ribosome (Fig. 1*J*). $Kras^{G12D}$ also induced genes encoding for *small nucleolar RNAs* (*snoRNAs*), which are known for their essential role in nucleolytic processing and *rRNA* maturation (*SI Appendix*, Fig. S1*I*) (23). To measure *rRNA* synthesis we used real-time qPCR to measure 47S pre-*rRNA* external transcribed spacers (ETSs), a proxy for the pre-*rRNA* transcriptional activity of *RNA* polymerase I (24). In accordance with the transcriptional profile, we observed accelerated *rRNA* production upon loss of *Apc* and the additional presence of $Kras^{G12D}$ (*SI Appendix*, Fig. S1*J*). The oncoprotein c-MYC is a well-known regulator of ribogenesis and highly expressed in Apc-deficient cells, where c-MYC expression can be further stabilized in a RAS-dependent manner (25, 26). Indeed, both c-MYC *mRNA* and protein levels in *Apc*-deleted cells were further increased upon additional $Kras^{G12D}$ (*SI Appendix*, Fig. S1 *K* and *L*). We also assessed how interfering with ribogenesis affected organoid growth, by treatment with actinomycin D (Act D) which blocks the activity of RNA polymerases at a low dose (27). Given that c-MYC directly controls activity of the RNA polymerases I and III (Pol I and III), resulting in induced *rRNA* synthesis essential for protein synthesis, mutant cells could be more sensitive to Pol inhibition (28). However, contrary to what we expected, we noticed that the growth of wild-type organoids, and to a lesser extend $Apc^{-/-}$ organoids, was strongly sensitive to nanomolar concentrations of actinomycin D, whereas growth of $Apc^{-/-}Kras^{+/G12D}$ organoids was strongly resistant to this (*SI Appendix*, Fig. S1 *M* and *N*). Thus, although mutations in *Apc* and *Kras* increase ribogenesis rates, the existence of a therapeutic window to specifically target this increase in ribogenesis remains to be determined.

In conclusion, loss of *Apc* and oncogenic $Kras^{G12D}$, associated with early adenomagenesis, enhances the global translational capacity of epithelial cells. This is accompanied by accelerated proliferation rates and expansion of the stem cell pool. Furthermore, both mutations synergistically induce a transcriptional program that results in increased c-MYC levels and activation of ribogenesis.

Reduced SMAD4 Expression Increases the Global Translational Capacity and Is Accompanied by Lower Levels of the CAP-Dependent Translational Repressor 4E-BP1. To extend these findings beyond genetic events associated with early adenomagenesis, we investigated the role of SMAD4. Inactivating mutations in TGFβ signaling components, including complete or partial loss of tumor suppressor SMAD4, correlate strongly with late-stage adenomas and the carcinoma transition phase (29). To include this in our model, we generated small intestinal organoids with constitutive knockdown using stable expression of short hairpin *RNAs* against *Smad4* (*shSmad4* organoids). This resulted in ∼50% reduction of *Smad4 mRNA* expression (*SI Appendix*, Fig. S2*A*). *shSmad4* organoids were resistant to BMP-mediated growth repression, as indicated by long-term culturing (>15 d) independent of BMP antagonist Noggin, showing that SMAD4 was functionally depleted (*SI Appendix*, Fig. S2*B*). When observing the growth of *shSmad4* organoids we noticed increased bud formation, suggestive of accelerated crypt formation (Movies S1 and S2). Accordingly, *mRNA* levels of *Lgr5*, *Ascl2*, *Olfm4*, as well as *Lyz1*, were elevated in *shSmad4* organoids, indicating enrichment of crypt-resident stem cells and Paneth cells (Fig. 2 *A* and *B*). We confirmed this by combining in situ hybridization for *Lgr5* and IHC for lysozyme (Fig. 2*C*). Expansion of stem- and Paneth cells in the crypt indeed strongly resembles the recently reported small intestinal phenotype of *Smad4* knockout mice (30). Interestingly, when comparing the global translational capacity of *shSmad4* organoids to organoids with the wild-type organoids transduced with a scrambled control *shRNA* (*shControl*), we observed a 30 to 40% increase (Fig. 2*D*). Withdrawal of Noggin from the culture medium of wild-type organoids resulted in a small but significantly declined global translation rate, indicating involvement of BMP signaling herein (*SI Appendix*, Fig. S2*C*).

To determine whether the higher global translational capacity following knockdown of *Smad4* was exerted by mechanisms additional to hyperactivation of WNT and RAS signaling, we introduced *Smad4* knockdown in cells with preexisting *Apc* and *Kras* mutations. Recombined $Apc^{-/-}Kras^{+/G12D}$ organoids were either transduced with a scrambled *shRNA*, from here on referred to as AK organoids, or *shRNAs* against *Smad4*, from here on referred to as AKS organoids. This organoid model is relevant, since mutations in the human *SMAD4* gene often mark late-stage events in carcinoma formation that follow preexisting mutations in *APC* and *KRAS* (31). As expected, AKS organoids grew completely independent of all medium growth factors (EGF, R-spondin, and Noggin) (32). Additional selection for reduced SMAD4 function was ensured using high-dose and long-term incubation with mouse recombinant TGFβ (33), which caused disintegration of AK organoids, whereas AKS organoids were completely resistant and showed clear regenerative potential after repassaging (*SI Appendix*, Fig. S2*D*). This effect has been described and involves the lack of SMAD4 which provides resistance to TGFβ/SMAD4-induced proapoptotic effects in the *Apc*-deficient stem cell (34). Interestingly, the clonogenic capacity, a functional stem cell property, was further increased in single cells derived from AKS organoids (Fig. 2*E*). Furthermore, *Smad4* knockdown in cells with mutations in *Apc* and *Kras* resulted in a higher global translational capacity (Fig. 2*F*).

To identify signaling transduction pathways related to regulation of global *mRNA* translation that were affected by *Smad4* knockdown, we compared the transcriptional profiles of AK and AKS organoids. Gene set enrichment analysis (GSEA) comparing gene sets from the Oncogenic Signatures database (Broad Institute), revealed that *Smad4* knockdown was associated with a transcriptional profile that matched a set (M2847) of up-regulated transcripts associated with cells with active eukaryotic translation initiation factor G1 (eIF4G1) (*SI Appendix*, Fig. S2*E*) (35). eIF4G is an essential translation initiation factor of the eIF4F complex, comprising the cap-binding protein eIF4E, the scaffold protein eIF4G, and the helicase eIF4A. This complex facilitates the interaction between the 43S-preinitiation complex and the capped *mRNA* (36). The entire complex is a critical regulatory nexus of dep-dependent translation initiation through upstream signaling pathways, including mTORC1 via eIF4E-binding protein 1 (4E-BP1) and RAS signaling via MNK1/2 (37). Upon hypophosphorylation, 4E-BP1 binds to eIF4E and prevents it from interacting with eIF4G to promote ribosome recruitment (38). Interestingly, recent reports have demonstrated that SMAD4 binds the promoter region of mouse and human *4EBP1*, stimulating translation initiation due to disinhibition of eIF4E (30, 39). In line with this observation, the transcriptome of AKS organoids was enriched for genes related to the gene set (M1919) of *Eif4ebp1*/*Eif4ebp2* double knockout mouse embryonic fibroblasts, cells that exhibit elevated protein synthesis rates (*SI Appendix*, Fig. S2*F*) (40). We thus hypothesized that knockdown of *Smad4* could reduce available 4E→BP1 levels that compete with eIF4G to bind and enhance the activity of eIF4E (41), which in turn would enhance cap-dependent translation activity (42). In support of this hypothesis, we found *mRNA* levels of both mouse homologs *4ebp1* and *4ebp2* to be reduced in *shSmad4* organoids (*SI Appendix*, Fig. S2 *G* and *H*). Moreover, 4E-BP1 protein expression was also at a reduced

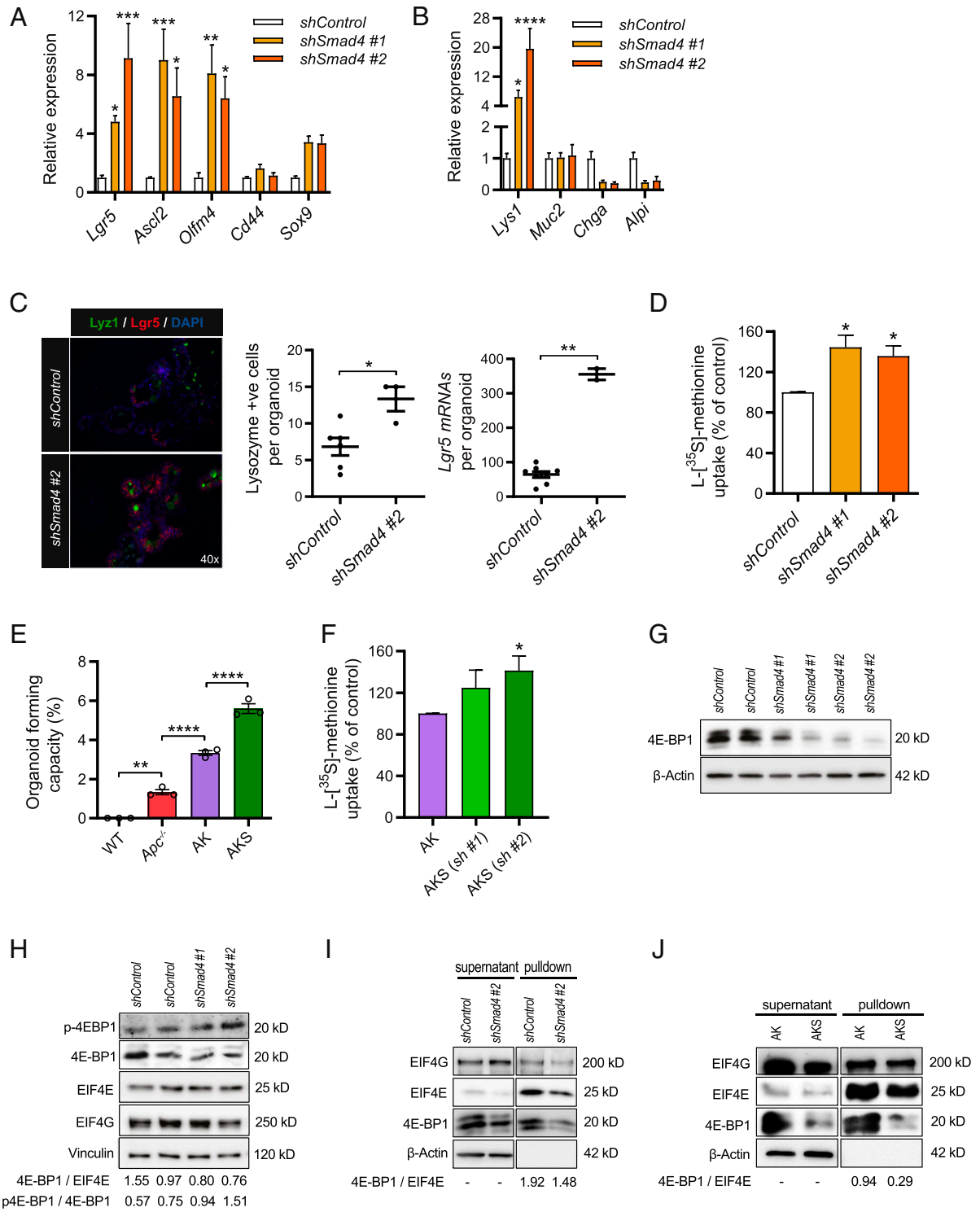

Fig. 2. Knockdown of Smad4 results in enrichment of the stem and Paneth cell compartments, which is accompanied by increased global translation and reduced expression of translational repressor 4E-BP1. (*A*) Quantitative RT-PCR analysis of crypt base columnar stem cell markers in *shSmad4* organoids ($n = 3$). (*B*) Analysis of small intestinal differentiation markers in *shSmad4* organoids ($n = 3$). (*C*) Combined staining of in situ hybridization of stem cell marker *lgr5* and immunostaining for Paneth cell marker lysozyme in *shSmad4* organoids, including quantification of the *mRNA* particles and lysozyme-positive cells per organoid. *$P < 0.05$, Student's *t* test. (*D*) L-[^{35}S]-methionine incorporation assay of *shSmad4* organoids assessed at day 4 after passaging ($n = 3$). (*E*) Clonogenic capacity of single cells that grow out to fully developed organoids, presented as a quantification of the organoid number per 20,000 seeded cells ($n = 3$). (*F*) L-[^{35}S]-methionine incorporation assay in *Apc*$^{-/-}$ *Kras*$^{+/G12D}$ *shSmad4#2* (AKS) and *Apc*$^{-/-}$ *Kras*$^{+/G12D}$ *shControl* (AK) organoids assessed at day 3 after passaging ($n = 4$). (*G*) Representative immunoblotting analysis of 4E-BP1 expression in *shSmad4* organoids. β-Actin served as a loading control ($n = 3$). (*H*) Representative immunoblotting analysis of phospho-4E-BP1 (Thr70), eIF4E, and eIF4G in *shSmad4* organoids. Optical density ratios of phospho-4E-BP1/4E-BP1 and 4E-BP1/eIF4E were also calculated ($n = 2$). (*I*) m7GTP-agarose pulldown assay in *shSmad4* organoids to assess the levels of cap-bound eIF4E, eIF4G, and 4E-BP1 ($n = 3$). Unbound levels of β-actin 4E-BP1 and eIF4G were detected in supernatants. (*J*) m7GTP-agarose pulldown assay comparing AKS (*shSmad4 #2*) to AK organoids (*shControl*) ($n = 3$). Data are represented as means ± SEM. Significance (one-way ANOVA) *$P < 0.05$, **$P < 0.01$, ***$P < 0.001$, ****$P < 0.0001$.

level in *shSmad4* organoids, while expression of the cap-binding proteins EIF4E and EIF4G were unchanged (Fig. 2 *G* and *H*). The ratio of 4E-BP1 to EIF4E was lower in *shSmad4* organoids, while any 4E-BP1 was largely phosphorylated (Fig. 2*H*). To show that less 4E-BP1 was bound to the cap-binding complex upon *Smad4* knockdown, we performed m7GTP pulldown assays in *shSmad4* organoids and quantified protein levels of bound 4E-BP1 relative to eIF4E. We consistently found relatively less 4E-BP1 bound to the *mRNA* cap, normalized to eIF4E, upon knockdown of *Smad4* in epithelial cells of wild-type and $Apc^{-/-}Kras^{+/G12D}$ backgrounds (Fig. 2 *I* and *J*). These data suggest that reduced SMAD4 levels could facilitate global translation via loss of 4E-BP1-mediated repression of functional eIF4E, increasing the cap-dependent translation efficiency.

Mouse and Human Epithelial Cells with Multiple Driver Mutations in *APC*, *KRAS*, *SMAD4*, and *TP53* Are Characterized by the Highest Capacity for Global Translation. To study a combination of all driver mutations related to the ACS, we continued investigating loss of p53, which hallmarks a majority of the metastasizing carcinomas (43). We first used small intestinal organoids isolated from $Trp53^{fl/fl}$ mice, which we subsequently transduced with the pRetro-MSCV-CreER^{T2} vector in order to obtain inducible $Trp53^{-/-}$ organoids. After in vitro recombination, *mRNA* levels of *Trp53* were undetectable and organoids proved completely insensitive to cell death induced by the MDM2-antagonist Nultin-3, confirming p53 loss of function (*SI Appendix*, Fig. S3 *A* and *B*). $Trp53^{-/-}$ organoids were undiscernible from non-recombined ($Trp53^{fl/fl}$) controls, and global translation rates were unaffected (Fig. 3*A*). However, upon pretreating $Trp53^{-/-}$ organoids with the GSK3β inhibitor CHIR-99021, which creates a condition of high WNT activity at the level of the β-catenin destruction complex that resembles deletion of *Apc*, global translation rates were significantly higher in $Trp53^{-/-}$ organoids (Fig. 3*B*). *Lgr5* was up-regulated, although expression of other WNT-related stem cell markers were unchanged in $Trp53^{-/-}$ cells (Fig. 3*C*). To further investigate the role of p53 in cells with the additional ACS mutations, we transduced *shRNAs* against *Trp53* in AKS organoids, from now on referred to as AKSP organoids (*SI Appendix*, Fig. S3*C*). AKSP organoids were resistant to simultaneously administered high-dose and long-term incubation with recombinant TGFβ and Nutlin-3 (*SI Appendix*, Fig. S3*D*). As expected, transcriptional profiling of AKSP cells was characterized by decreased expression of a large set of proapoptotic genes (*SI Appendix*, Fig. S3*E*). Strikingly, we found that the global translational capacity in AKSP organoids was even further elevated (Fig. 3*D*). To assess if these findings are relevant in the setting of human colon epithelium, we used previously published genetically engineered colon organoids with mutations in the *APC*, *KRAS*, and *TP53* genes (32). Here we observed a pattern similar to murine small intestinal cells, where the global translational capacity was highest in colonic cells with quadruple driver mutations (Fig. 3*E*). To further validate this in human CRC cells that carry naturally occurring oncogenic mutations, we analyzed the global translation rate of patient-derived tumor organoids that were previously characterized (44, 45). Again, tumor cells with multiple driver mutations in *APC*, *KRAS*, *SMAD4*, and *TP53* harbored the highest global translational capacity, indicating that each of these mutations controls global translation in CRC cells (Fig. 3*F*).

Increased Proliferation and Growth Can Be Targeted by Interfering with Global mRNA Translation Via mTOR Signaling or the Function of Downstream eIF4E. Sustained global translation provides the biosynthetic needs for cell growth, which explains why these biological processes are often linked, at least in immortalized mammalian cell lines (42). To assess whether the parameters of global translation, growth, and proliferation are correlated in intestinal epithelial cells, we seeded single cells from AK, AKS, and AKSP organoids and quantified growth over time. AKSP organoids grew exceptionally fast, reaching their optimal size in as fast as 3 d, exceeding the rate of AKS and AK organoids (Fig. 4*A*). Proliferation rates, as measured by incorporation of 5-ethynyl-2′-deoxyuridine (EdU) in the S phase, were also highest in AKSP organoids, demonstrating that global translation, cell division, and growth remain associated during oncogenic transformation (Fig. 4*B*). *mRNA* translation and proliferation are likely to be codependent processes, in which translation rates are adjusted to meeting the demands of proliferation (46–48). However, whether enhanced rates of global translation due to the concerted action of multiple driver mutations enables greater proliferation, and whether there exists a window to inhibit this process by selectively targeting the translational apparatus, remains to be determined. To address this, we directly blocked global translation at the level of initiation or elongation and measured the effect on cellular proliferation, using ribavirin and cycloheximide. After short-term exposure to both inhibitors, proliferation was already strongly reduced, indicating that global translation is required for these cells to divide (*SI Appendix*, Fig. S3 *F* and *G*). Next, we aimed to identify which signaling transduction pathways involved in control of global translation were activated during the ACS. To this end we compared transcriptional profiles of each organoid genotype, and looked for genes that follow a stepwise increase, similar to the relative increase in global translation rates, using R2 software. Unbiased pathway analysis on the resulting list of genes revealed that mTOR signaling components were overrepresented ($P = 6.1 \times 10^{-6}$). mTOR is a pivotal cellular transduction pathway that coordinates eukaryotic cell growth and metabolism with environmental inputs, by regulating global translation via several downstream effector kinases (*SI Appendix*, Fig. S3*H*) (49). Moreover, when looking at a set of previously described genes related to glucose metabolism that are transcriptionally regulated by mTORC1 (50), a pattern of increased expression was observed, suggesting mTORC1 hyperactivation throughout the ACS (Fig. 4*C*). We examined the posttranslational phosphorylation status of the target effector proteins RPS6 and 4EBP1, which can be phosphorylated by mTORC1 (49). In line with the transcriptional data, levels of phosphorylated RPS6 (Ser240/244 and Ser235/236) were increased upon accumulation of ACS mutations (Fig. 4*D*). On the other hand, expression levels of phosphorylated 4E-BP1, which are initially up-regulated in the context of *Apc* loss, are subsequently extinguished by additional mutations in *Kras*, *Smad4*, and *P53*. This was paralleled by loss of total 4EBP1 levels, which are undetectable in AKS and AKSP organoids (Fig. 4*D*). Interestingly, similar observations of lost 4EBP1 expression were seen in tissue of progressed human pancreatic cancers, tumors hallmarked by mutations in *KRAS*, *SMAD4*, and *TP53* (51). Thus mTORC1 signaling may drive global translation during oncogenic transformation throughout the ACS, potentially steering growth and proliferation of intestinal epithelial cells as a consequence.

To assess the vulnerability to mTOR inhibition and the effects on growth, we used multiple mTOR inhibitors that vary in specificity and potency (52). First we tested rapamycin, a well-studied compound that inhibits mTORC1/S6K signaling, and has been proven effective in CRC mouse models with loss of APC, although tumor cells with high RAS signaling due to additional mutations in *KRAS* or *PIK3CA* have been proven rapamycin insensitive (9, 53, 54). We indeed found that rapamycin affected epithelial cells with loss of *Apc*, consistent with previous literature, but had little to no effect on growth of AK and AKS organoids, respectively (*SI Appendix*, Fig. S3*I*) (9). We then used Torin1, a more potent inhibitor of mTORC1, that possesses dual effectiveness in blocking both the mTORC1/S6K and mTORC1/4E-BP1 effector branches of the pathway (49, 55). Interestingly, contrary to rapamycin, Torin1 was able to also inhibit growth of cells with multiple ACS mutations, indicating that these cells remain dependent on activation of mTORC1 signaling (Fig. 4*E*

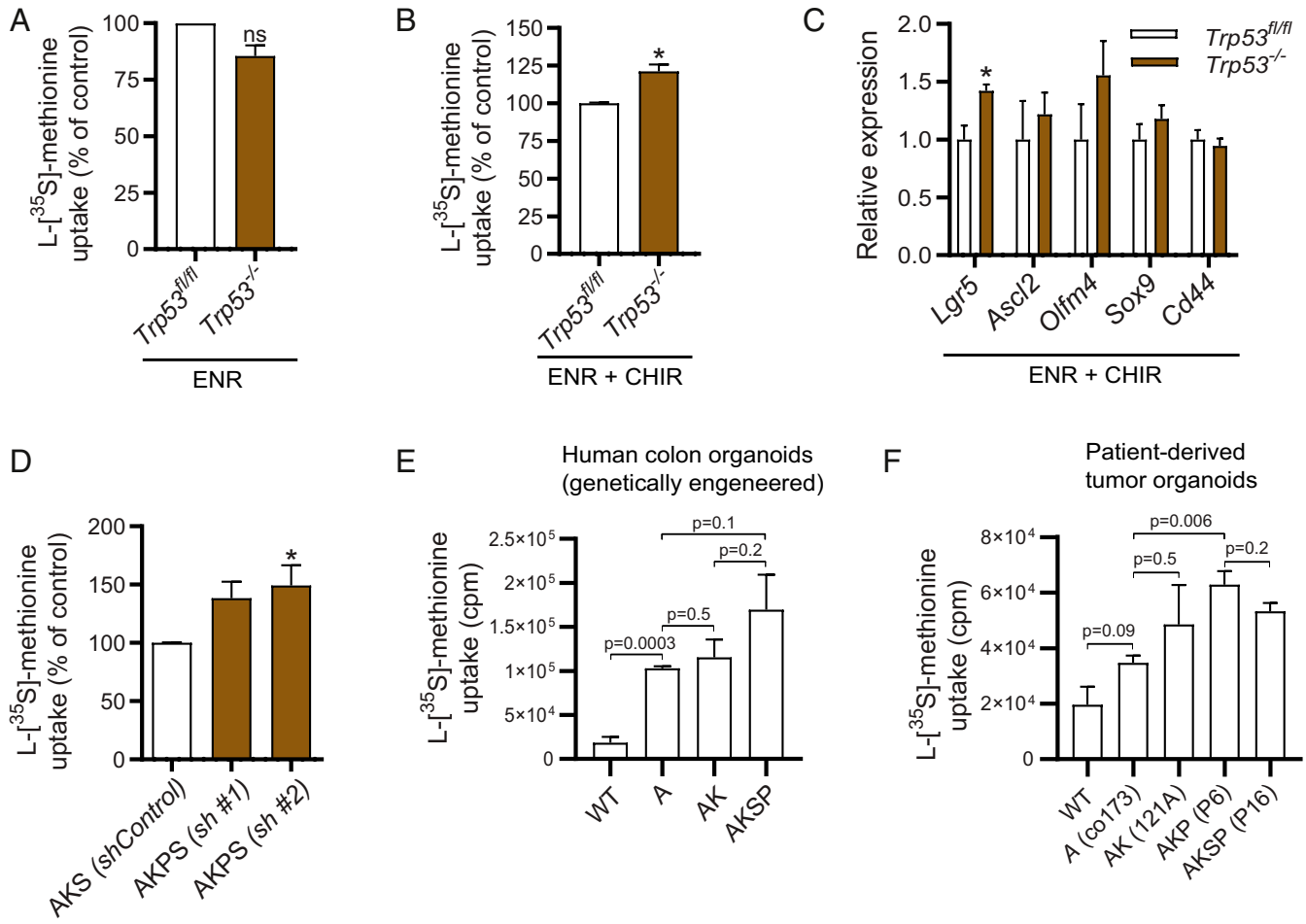

Fig. 3. A combination of mutations in APC, KRAS, SMAD4, and TP53 results in the highest global translational capacity in mouse small intestinal organoids, human colon organoids, and patient-derived tumor organoids. (*A*) L-[^{35}S]-methionine incorporation assay of MSCV-Cre *Trp53*$^{-/-}$ organoids assessed at day 3 after passaging in ENR ($n = 3$). (*B*) L-[^{35}S]-methionine incorporation assay of MSCV-Cre *Trp53*$^{-/-}$ organoids assessed at day 3 after passaging pretreated for 96 h in ENR with 5 μM CHIR-99021 ($n = 3$). (*C*) Quantitative RT-PCR analysis of crypt base columnar stem cell markers in MSCV-Cre *Trp53*$^{-/-}$ organoids ($n = 3$). One-way ANOVA. (*D*) L-[^{35}S]-methionine incorporation assay of AKSP compared to AKS organoids assessed at day 3 after passaging ($n = 4$). (*E*) L-[^{35}S]-methionine incorporation assay in genetically engineered human colon organoids with mutations in *APC*, *KRAS*, *SMAD4*, and *TP53* as previously described (32). ($n = 3$) (*F*) L-[^{35}S]-methionine incorporation assay in FAP patient-derived organoids (co173, 121A) and sporadic CRC tumor organoids (P6, P16) that carry mutations in *APC*, *KRAS*, *SMAD4*, and *TP53* as previously described ($n = 3$) (37, 38). FAP, familial adenomatous polyposis; counts per minute (cpm), cpm relative to protein biomass. Data are represented as means ± SEM. Significance (Student's *t* test/one-way ANOVA) *$P < 0.05$. ns, not significant.

and *SI Appendix*, Fig. S3*J*). Moreover, sensitivity to Torin1 corresponded with a stepwise reduction in *mRNA* expression of stemness marker *Lgr5* (*SI Appendix*, Fig. S3*K*). Because we observed reduced 4E-BP1 interaction to the cap-binding complex in our cancer models with knockdown of *Smad4*, we examined the effect of inhibiting functional eIF4E using ribavirin, a pharmacological 4E-BP1 mimetic (56). Strikingly, after dose titration, we identified a therapeutic window at which the growth of wild-type and *Apc*-deficient organoids was relatively unaffected, whereas AK, AKS, and AKSP organoids were increasingly more susceptible (Fig. 4*F* and *SI Appendix*, Fig. S3*L*). Most notable was the effect of ribavirin on growth of AKSP organoids that carry quadruple mutations (Fig. 4*F*). It was previously reported that growth of cancer cells with high eIF4E expression, including breast cancer and leukemia cell lines, were increasingly ribavirin sensitive (56, 57). In line with these studies, we observed elevated baseline *mRNA* and protein expression levels of eIF4E in our ACS organoid models (Fig. 4*G*). Collectively, our data thus demonstrate increased global translation enables proliferation and growth of cells with triple and quadruple ACS mutations, via a deliberate and targetable increase in downstream mTORC1 target eIF4E.

Discussion

Deregulated translational control is considered to be a crucial component in various cancers, although not much is known about CRC in this respect. We set out to investigate the role of key oncogenic driver mutations on the global translational capacity of intestinal epithelial cells. Using various murine and human intestinal organoid models, we show that global translation can be strongly enhanced upon the acquisition of mutations in the genes for *APC*, *KRAS*, *SMAD4*, and *TP53*. Activated WNT signaling by deletion of *Apc* appears to be a prerequisite for *Kras*^{G12D} to further increase global translation and proliferation. Indeed, synergic mechanisms operating between WNT and RAS signaling have been reported (58, 59). In mice, transgenic *Kras*^{G12D} alone is insufficient to initiate tumor formation, but it significantly promotes CRC formation and progression in an *Apc*-deleted background (19, 53, 58, 59). Whether enforced global translation is actually required to exert the oncogenic potential of *Kras*^{G12D} in cells is an issue that warrants further

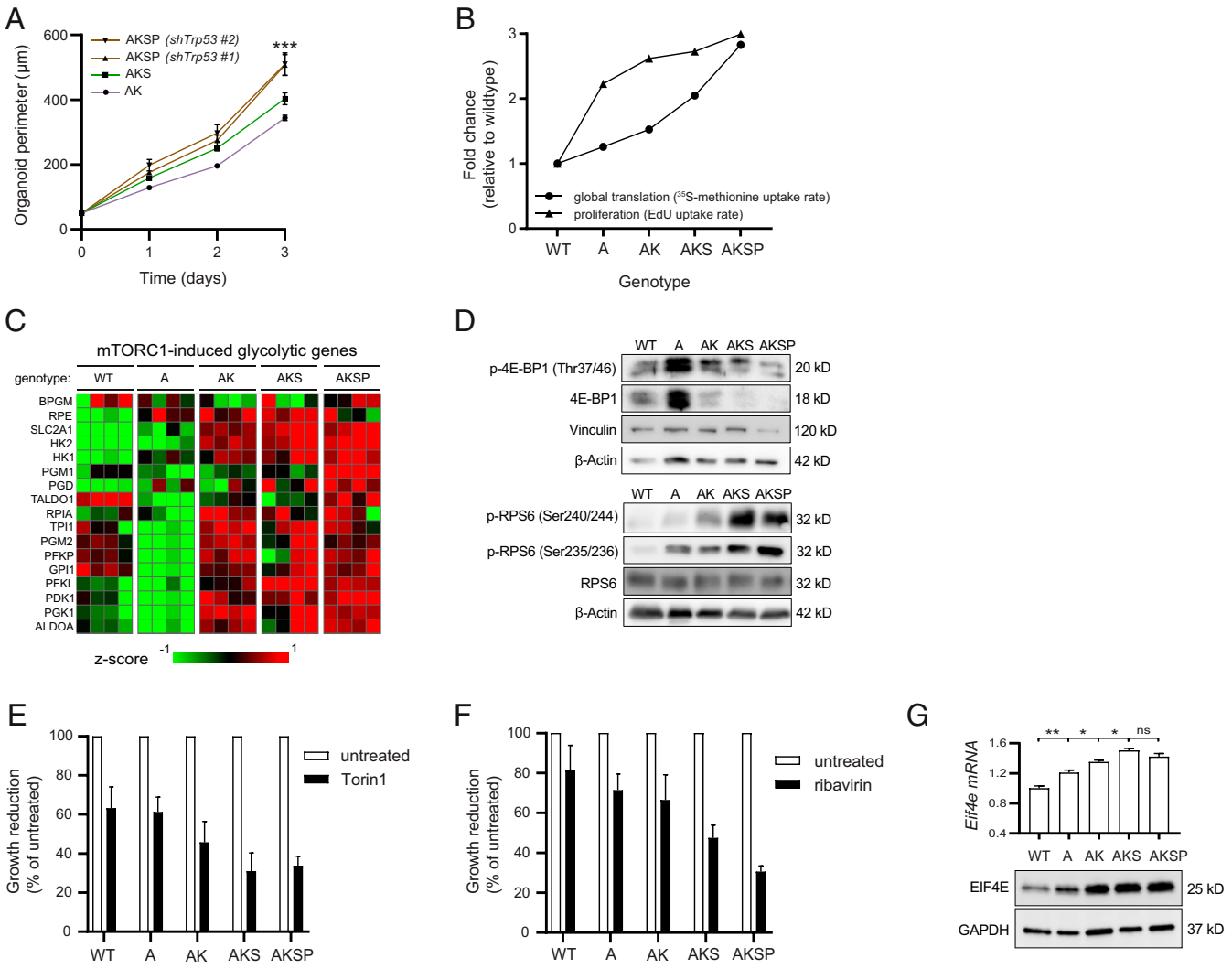

Fig. 4. High global translational capacity enables growth in cells with multiple ACS mutations in a mTOR/eIF4E-dependent manner. (*A*) Representative time curve of organoid growth starting from 10,000 single-seeded cells and grown for 3 d. Quantified as mean organoid perimeter per well, four wells per condition ($n = 2$). (*B*) Plotted rates of global translation (from L-[^{35}S]-methionine incorporation assays), and proliferation (from EdU incorporation assays), in organoids of all ACS genotypes. Data are presented as fold change relative to the proliferation and translation rate of wild-type organoids. (*C*) Heatmap of microarray *mRNA* expression data in organoid of all ACS genotypes, containing a subset of transcriptional target genes associated with mTOR signaling described previously (50). ($n = 4$). (*D*) Western blotting analysis of phosphorylated and total 4E-BP1 and RPS6, effectors downstream of mTORC1 signaling. (*E*) Quantification of growth in organoids treated for 48 h with 50 nM Torin 1 and presented as the growth reduction after treatment in each genotype relative to untreated controls ($n = 4$). (*F*) Quantification of growth in organoids treated for 48 h with 10 µM ribavirin and presented as the growth reduction after treatment in each genotype relative to untreated controls ($n = 3$). (*G*) Western blotting analysis of EIF4E levels in organoid of all ACS genotypes as well as *mRNA* expression levels derived from the microarray analysis. Data are represented as means ± SEM. Significance (one-way ANOVA) $*P < 0.05$, $**P < 0.01$, $***P < 0.001$. ns, not significant.

investigation. With regards to (partial) loss of SMAD4 and p53, we observed that both events can act as enhancers of the global translational capacity. Interestingly, synergy in terms of their oncogenic potential has been reported between these driver mutations as well (60, 61). It is plausible that deregulated global translation, through the cross-talk of multiple oncogenic pathways, is the main determinant of sustaining the cancer cell proteome. APC and KRAS may facilitate this process by activation of ribogenesis, through stabilizing the activity of c-MYC (25). Additional loss of SMAD4, via reduced 4E-BP expression, could unleash maximal efficiency of eIF4E-mediated cap-dependent translation of tumorigenic *mRNAs* that promotes oncogenic transformation (62). Loss of p53, which we have not further assessed here, could be crucial for cancer cells to cope with prolonged proteotoxic stress that arises from processing nascent polypeptides by preventing apoptosis (63), allowing high expression of oncogenes such as c-MYC (64).

It remains challenging to interfere therapeutically with global translation in cancer cells, without affecting healthy cell function concurrently. We first tried to indirectly modulate global translation by inhibition of ribogenesis using a Pol1 inhibitor. However, this was not possible without significantly retarding growth of wild-type cells too, probably because the therapeutic window was too narrow for partial suppression of ribogenesis. Secondly, because we found hyperactivated mTORC1 signaling, we tried to modulate global translation by blocking mTORC1 function and assess organoid growth. However, additional mutations in *Kras* and *Smad4* conferred rapamycin resistance in *Apc*-deficient cells, possibly due to lower 4E-BP1/eIF4E ratios, which has been described to be a determinant for responsiveness in other cancers

(65, 66). Furthermore, rapamycin has a differential effect on 4E-BP1 versus S6K, and cap-dependent translation can be maintained through 4EBP1 phosphorylation (67). Torin1 on the other hand, a more potent inhibitor that also suppresses rapamycin-resistant functions of mTORC1 that are necessary for cap-dependent translation (68), could effectively inhibit growth of cells with ACS mutations, although we found wild-type cells to be sensitive too. Since we found lower ratios of 4E-BP1/eIF4E in triple mutant cells, we reasoned that directly interfering with the eIF4G-eIF4E interaction using the 4E-BP1 mimetic ribavirin could be effective. Indeed, we identified a therapeutic window of opportunity where selectively impeding with cap-dependent translation initiation predominantly affected quadruple mutant cells, while minimal effect on wild-type cells was seen. *Apc*-deficient cells were also relatively insensitive to ribavirin in these concentrations, potentially because these cells rely primarily on increased translation elongation rather than initiation (9). However, our results point toward a central role for translation initiation at later stages during the ACS, which suggests that adenocarcinoma cells might not be able to fully circumvent cap-dependent translation by alternative modes of initiation (69).

A few points of discussion must be mentioned with regards to this study. First of all, since the role of SMAD4 and p53 was partly assessed using noninducible siRNA strategies, the nature of these models did not allow us to examine any direct effects of complete loss of function, although these models are still relevant (70). Gene dosage and temporal aspects associated with knockdown strategies may have a significant effect, as they gradually change the distribution of cell types in the multicellular organoids, and thus the global translational capacity that is measured. Second of all, relation between global translation and proliferation in organoids was nonlinear. This may be explained by different cell ratios in a multicellular system, particularly after introducing a deletion in *Apc*, which is known to enrich the number of activated stem cells at the cost of differentiated cells. Better techniques for accurate single cell measurement of global translation in organoids must delineate how different intestinal cell types harbor different translational capacities. Third, an important caveat of using in vitro epithelial organoid culture systems to study global translation is that the effects of non-epithelial cells remain unknown. The cellular context normally provided by stroma and immune cells, as well as nutrient deficiency due to poorly vascularized tumor regions, will likely have a major impact on cancer cell behavior, including translation and proliferation. Additional research will unravel the degree of dependency on global translation of CRC cells in vivo, in order to explore the feasibility of developing treatment strategies that specifically target the translational apparatus in CRC. Because *mRNA* translation is such an energetically expensive process, future research should also address how cancer cells meet the high metabolic demands of global translation (71).

Materials and Methods

Generation and Culture of Organoids. All experiments were approved by the relevant local ethical committees. When experimental tissue from human subjects were used informed consent was obtained and the study was approved by the ethical committee. Mouse small intestinal organoids were generated according to methods previously described (72). Organoids were cultured in media containing N2, B27 supplements (Invitrogen), 1.25 mM n-acetylcysteine, 50 ng/mL mouse EGF (Invitrogen), Noggin-Fc-conditioned medium (20%, equivalent to 200 ng/mL), and Rspo1-Fc-conditioned medium, unless specifically stated otherwise. Noggin-Fc-conditioned medium was obtained through collection of supernatant from HEK293T cells transfected with a Noggin-Fc expression vector as previously described (73). Human genetically engineered colon organoids (32), familial adenomatous polyposis (FAP) patient-derived organoids (44), and tumor organoids from CRC patients (45), were cultured in mouse small intestinal organoid medium with addition of 2-mercaptoethanol (Sigma-Aldrich), gentamicin (BioWhittaker), 50 mM TGF-βRI inhibitor A38-01 (Tocris Bioscience), 30 mM p38 inhibitor SB202190 (Sigma-Aldrich), and 500 μM (Leu15)-gastrin (Sigma-Aldrich).

Experiments with inducible organoids using the Villin-Cre^{ER} system were performed on a C57BL/6J background. In vitro Cre-mediated recombination was achieved using 0.75 μg/mL 4-hydroxy tamoxifen for 24 h. Organoids with mutations in *APC*, *KRAS*, and *TP53* were derived from previously published *Apc*$^{580S/580S}$ conditional mice, *Kras*$^{+/G12D}$ conditional mice, and *Trp53*$^{F2\text{-}10/F2\text{-}10}$ conditional mice, respectively (74–76). AKS and AKSP organoids were generated by stable lentiviral cotransduction of two short hairpin *RNAs* against *Smad4* and *Trp53* in *Apc*$^{-/-}$*Kras*$^{+/G12D}$ organoids, according to previously described methodology (77, 78). Subsequently, selection for mutated cells was performed using growth factor depletion from the culture medium (EGF depletion to select for *Kras*$^{+/G12D}$ cells, R-spondin depletion to select for *Apc*$^{-/-}$ cells, and Noggin depletion to select for cells with knockdown of *Smad4*). A 5-d incubation with (±)-Nutlin-3 (10 μM, Cayman Chemical) was used to select for cells with knockout and knockdown of *Trp53*. Knockdown of *Smad4* in *Apc*$^{-/-}$*Kras*$^{+/G12D}$ organoids was achieved by at least a 7-d incubation with recombinant human TGFβ (10 ng/mL, Bioscience).

Quantification of organoid growth was done by microscopic assessment of individual organoids that were cultured in a 48-well plate, by measuring the perimeter or area with ImageJ software. In quantifications presented in the figures, each biological replicate consists of the mean quantified growth of three wells.

Clonogenicity Assay. We assessed the clonogenic potential of single cells from organoids. Briefly, organoids were grown up to 4 d before repassaging. First Matrigel was fractionated using a narrowed Pasteur pipette and consequently removed through centrifuging (800 rpm). Crypts were dissociated to single cells after 10 min of 37 °C incubation with TrypLE (Gibco). The absolute number of cells per condition was equalized using a Beckman Coulter particle counter (Z-series). For each condition, 20,000 cells in 20 μL Matrigel were seeded per well (three wells) and the number of outgrowing organoids was quantified after 3 to 5 d.

Assessment of Global Translation. To measure all newly synthesized proteins, we quantified the incorporation of ^{35}S-labeled methionine and cysteine in organoids. Organoids were grown for 3 to 4 d after passaging and seeded into 48-well plates. In the experiments using human organoids, growth factors (EGF, Noggin, and R-spondin) and TGFβ and p38 inhibitors were depleted for 48 h prior to the assay.

After a 15-min starvation period to deplete endogenous methionine, cells were exposed to a pulse phase of 45 min to label all newly synthesized proteins using 1 μL (1.25 μCi/mL) of EasyTag L-[^{35}S]-methionine (PerkerElmer) per well at 37 °C, 95% humidity, and 5% CO_2 conditions. Organoids were then washed two times in cold PBS, harvested, and spun down in cold PBS to remove supernatant and any Matrigel fragments. Cell pellets were lysed in cell lysis buffer (Cell Signaling Technology) and spun down to remove any unresolvable phospholipids. A 15-μL aliquot of radioactive lysate was blotted on labeled 24-mm diameter glass microfiber filters (GF/C Whatman) that were presoaked in 20% trichloroacetic acid (TCA). Filters were replaced in a vacuum manifold and incubated in 10% ice cold TCA for another 15 min, followed by 10% TCA at 90 °C for 8 min to break any aminoacyl-tRNA bonds. Filters were washed twice in 2% TCA and twice in 96% ethanol. Air dried filters (>20 min) were incubated in liquid scintillation mixture (Ultima Gold, PerkerElmer) for 2 h and radioactive disintegration per minute (dpm) was quantified using a scintillation counter (Tri-Carb 2900TR, PerkerElmer). Counts were presented as percentage relative to control samples, after normalization to total protein, using bicinchoninic acid assay according to manufacturer's instructions (BCA Protein Assay Kit, Pierce).

Alternatively, incorporation of AHA-labeled methionine was used to label newly synthesized protein according to manufacturer's instructions (AHA Click-it kit for Alexa Fluor 488, Thermo Fisher). Fluorescence was quantified on a flow cytometer (LSR Fortessa) and analyzed with FlowJo 8.0 software.

Assessment of Proliferation. To assess proliferation in organoids, we used BrdU labeling for DNA synthesis and S phase analysis. Organoids were incubated with 10 μg/mL BrdU 2 h before harvesting for paraffin embedding and immunohistochemistry using a mouse anti-BrdU antibody (11170376001, Roche). Alternatively, EdU staining was performed to analyze cell proliferation by flow cytometry using the Click-iT EdU Alexa Fluor 647 kit (Invitrogen). In some experiments, 2 h of 10 μg/mL cycloheximide (Sigma-Aldrich) or 4 h of 1 mM ribavirin (Sigma-Aldrich) was added prior to and during the labeling step. Organoids were incubated with 10 μM EdU for 4 h followed by TrypLE-mediated cell dissociation. Cell were fixated for 20 min with 3.7% formaldehyde, washed, and incubated with Click-iT reaction mixture according to the

manufacturer's protocol. Fluorescence was quantified on a flow cytometer (LSR Fortessa) and the percentage of EdU-positive cells was calculated with FlowJo 8.0 software.

RNA Extraction and RT-qPCR. All organoids were harvested at the indicated times, and *RNA* was extracted using the ISOLATE II *RNA* Mini Kit (BIO-52073, Bioline). cDNA was synthesized from 1 μg of purified *RNA* with Oligo-dT primer and Random Hexamers Primer using Revertaid reverse transcriptase according to protocol (Fermentas). Quantitative RT-PCR was performed using sensifast SYBR No-ROX Kit (GC-biotech Bio-98020) according to the manufacturer's protocol on a BioRad iCycler.

In Situ Hybridization. *RNA*scope experiments were performed using *RNA*-scope, an *RNA* in situ hybridization technique. *RNA*scope was performed according to the "Formalin-Fixed Paraffin-Embedded (FFPE) Sample Preparation and Pretreatment for RNAscope 2.5 assay" and "RNAscope 2.5 HD Detection Reagent—RED" protocols as provided by the manufacturer.

Microarray Analysis. Organoids were grown to day 3 and *RNA* was harvested as described above. A total of 400 ng of purified *RNA* was amplified and labeled using the 3′ IVT Pico Kit (Affymetrix) and *RNA* Amplification Kit (Nugene) according to manufacturers' protocols. Microarray analysis of mouse organoids was performed using Affymetrix Clariom S mouse array by the Dutch Genomics Service and Support Provider (MAD, Science Park, University of Amsterdam, The Netherlands). Washing and staining were performed by the GeneChip Fluidics Station 450 and the scanning was performed using the GeneChip Scanner 3000 7G (both Thermo Fisher Scientific). Data normalization, statistical testing, and extraction of differentially expressed genes was performed using the R2 platform. A complete description of the bioinformatics tool R2 may be found at https://hgserver1.amc.nl/cgi-bin/r2/main.cgi.

Immunoblotting. Cells were lysed in cell lysis buffer (Cell Signaling Technology) and heated to 95 °C for 5 min in sample buffer containing 0.25 M Tris·HCl (pH 6.8), 8% sodium dodecyl sulfate (SDS), 30% glycerol, 0.02% bromophenol blue, and 1% β-mercaptoethanol. Separation was done on 6 to 12% SDS/polyacrylamide gel electrophoresis (PAGE), and proteins were transferred to a polyvinylideenfluoride membrane. Specific detection was done by incubating the blot overnight in Tris-buffered saline (TBS) with 0.1% Tween-20 and 1% bovine serum albumin (BSA). Antibody binding was visualized using the Lumi-Light Western blotting substrate (Roche). Bands were quantified using ImageJ software. Antibodies are as follows: β-Actin (Sigma, Ab1978), Vinculin (Cell Signaling, 18799S), GAPDH (Cell Signaling, 2118S), 4E-BP1 (Cell Signaling, 9644), p4E-BP1 Thr37/46 (Cell Signaling, 2855), EIF4E (Cell Signaling, 9644), EIF4G (Cell Signaling, 8701), pS6 (Cell Signaling, 4857S), and c-MYC (Santa Cruz, sc-764).

Immunohistochemistry. Organoids were fixed overnight in 4% formaldehyde, embedded in paraffin, and sectioned. For staining, sections were deparaffinized with xylene and gradually rehydrated in ethanol. After blocking the endogenous peroxidase (0.01% H2O2 in methanol), slides were boiled for 20 min at 100 °C on a heat block in 0.01 M sodium citrate buffer (pH 6) for antigen retrieval. Slides were incubated overnight with primary antibody diluted in phosphate buffered saline (PBS) with 1% BSA and 0.1% Triton X-100. Powervision secondary antibody (Immunologic) was added for 30 min followed by incubation with detection antibody. Antibody binding was visualized by adding chromagen substrate diaminobenzedine (Sigma-Aldrich) according to the manufacturer's protocol. Antibody used was Muc2 (Santa Cruz, sc-15334).

m7GTP Pulldown Assay. Organoids from 24 wells of a 48-well plate were pooled and pellets were lysed in buffer containing 10 mM Tris·HCl (pH 7.6), 140 mM KCL, 4 mM $MgCl_2$, 1 mM dithiothreitol, 1 mM ethylenediaminetetraacetic acid, 1% Nonidet P-40, 1 mM phenylmethylsulfonyl fluoride, Complete Protease Inhibitor Mixture (Roche), 0.2 mM sodium orthovanadate. 30 to 50 μL of 7-methyl-GTP-agarose beads (Immobilized γ-Aminophenyl-m7GTP-C10-spacer, Jena Bioscience) was added and samples were incubated overnight. After washing two times in lysis buffer and two times in PBS, beads were resuspended in 1× SDS loading buffer. Samples were loaded on 6% gradient SDS/PAGE gel and immunoblotted for EIF4E and 4E-BP1. Quantification of the 4E-BP1/EIF4E ratio was calculated using ImageJ software.

Statistical Analysis. Statistical analysis was performed using Prism 8.0 (GraphPad Software). All values are represented as the mean ± SEM. Statistical tests are indicated in the figure legends. All experiments were performed as biological triplicates unless specifically stated otherwise. *P* value <0.05 was considered statistically significant.

Data Availability. All of the microarray data shown in the manuscript and *SI Appendix* are deposited in the Gene Expression Omnibus Database (GSE143509).

ACKNOWLEDGMENTS. We thank professor Owen Sansom of the Cancer Research UK Beatson Institute for kindly providing mouse small intestinal inducible $Apc^{580S/580S}$ and $Kras^{+/G12D}$ organoids. This work was supported in part by grants of the Amsterdam Medical Center PhD scholarship 2015, Dutch Cancer Foundation (KWF/UVA 2013-6135 and KWF/Alpe 11053/2017-1), and by a grant from the Netherlands Organization for Scientific Research (NWO-Veni 91615032).

1. E. R. Fearon, B. Vogelstein, A genetic model for colorectal tumorigenesis. *Cell* **61**, 759–767 (1990).
2. L. D. Wood *et al*., The genomic landscapes of human breast and colorectal cancers. *Science* **318**, 1108–1113 (2007).
3. R. Jackstadt, O. J. Sansom, Mouse models of intestinal cancer. *J. Pathol.* **238**, 141–151 (2016).
4. D. Silvera, S. C. Formenti, R. J. Schneider, Translational control in cancer. *Nat. Rev. Cancer* **10**, 254–266 (2010).
5. J. Chu, M. Cargnello, I. Topisirovic, J. Pelletier, Translation initiation factors: Reprogramming protein synthesis in cancer. *Trends Cell Biol.* **26**, 918–933 (2016).
6. A. G. Bader, P. K. Vogt, An essential role for protein synthesis in oncogenic cellular transformation. *Oncogene* **23**, 3145–3150 (2004).
7. M. L. Truitt, D. Ruggero, New frontiers in translational control of the cancer genome. *Nat. Rev. Cancer* **16**, 288–304 (2016).
8. C. Tomasetti, L. Marchionni, M. A. Nowak, G. Parmigiani, B. Vogelstein, Only three driver gene mutations are required for the development of lung and colorectal cancers. *Proc. Natl. Acad. Sci. U.S.A.* **112**, 118–123 (2015).
9. W. J. Faller *et al*., mTORC1-mediated translational elongation limits intestinal tumour initiation and growth. *Nature* **517**, 497–500 (2015).
10. J. F. van Lidth de Jeude *et al*., Heterozygosity of chaperone Grp78 reduces intestinal stem cell regeneration potential and protects against adenoma formation. *Cancer Res.* **78**, 6098–6106 (2018).
11. B. Schwanhäusser *et al*., Global quantification of mammalian gene expression control. *Nature* **473**, 337–342 (2011).
12. F. Loayza-Puch *et al*., p53 induces transcriptional and translational programs to suppress cell proliferation and growth. *Genome Biol.* **14**, R32 (2013).
13. V. Korinek *et al*., Constitutive transcriptional activation by a beta-catenin-Tcf complex in APC-/- colon carcinoma. *Science* **275**, 1784–1787 (1997).
14. L. E. Dow *et al*., Apc restoration promotes cellular differentiation and reestablishes crypt homeostasis in colorectal cancer. *Cell* **161**, 1539–1552 (2015).
15. D. J. Huels, O. J. Sansom, Stem vs non-stem cell origin of colorectal cancer. *Br. J. Cancer* **113**, 1–5 (2015).
16. W. De Roock *et al*., Effects of KRAS, BRAF, NRAS, and PIK3CA mutations on the efficacy of cetuximab plus chemotherapy in chemotherapy-refractory metastatic colorectal cancer: A retrospective consortium analysis. *Lancet Oncol.* **11**, 753–762 (2010).
17. E. R. Fearon, Molecular genetics of colorectal cancer. *Annu. Rev. Pathol.* **6**, 479–507 (2011).
18. J. H. van Es *et al*., Notch/γ-secretase inhibition turns proliferative cells in intestinal crypts and adenomas into goblet cells. *Nature* **435**, 959–963 (2005).
19. Y. Feng *et al*., Mutant KRAS promotes hyperplasia and alters differentiation in the colon epithelium but does not expand the presumptive stem cell pool. *Gastroenterology* **141**, 1003–1013–10 (2011).
20. S. C. Dolfi *et al*., The metabolic demands of cancer cells are coupled to their size and protein synthesis rates. *Cancer Metab.* **1**, 20 (2013).
21. I. Topisirovic, N. Sonenberg, mRNA translation and energy metabolism in cancer: The role of the MAPK and mTORC1 pathways. *Cold Spring Harb. Symp. Quant. Biol.* **76**, 355–367 (2011).
22. N. T. Ingolia, L. F. Lareau, J. S. Weissman, Ribosome profiling of mouse embryonic stem cells reveals the complexity and dynamics of mammalian proteomes. *Cell* **147**, 789–802 (2011).
23. D. Tollervey, T. Kiss, Function and synthesis of small nucleolar RNAs. *Curr. Opin. Cell Biol.* **9**, 337–342 (1997).
24. A. Popov *et al*., *Duration of the First Steps of the Human rRNA Processing*, (Nucl., United States, 2013).
25. J. van Riggelen, A. Yetil, D. W. Felsher, MYC as a regulator of ribosome biogenesis and protein synthesis. *Nat. Rev. Cancer* **10**, 301–309 (2010).
26. R. Sears, G. Leone, J. DeGregori, J. R. Nevins, Ras enhances Myc protein stability. *Mol. Cell* **3**, 169–179 (1999).
27. M. Girard, S. Penman, J. E. Darnell, The effect OF actinomycin ON ribosome formation IN hela cells. *Proc. Natl. Acad. Sci. U.S.A.*, 10.1073/pnas.51.2.205 (1964).
28. K. J. Campbell, R. J. White, MYC regulation of cell growth through control of transcription by RNA polymerases I and III. *Cold Spring Harb. Perspect. Med.* **4**, a018408 (2014).

29. P. W. Voorneveld, R. J. Jacobs, L. L. Kodach, J. C. H. Hardwick, A meta-analysis of SMAD4 immunohistochemistry as a prognostic marker in colorectal cancer. *Transl. Oncol.* **8**, 18–24 (2015).
30. Z. Qi *et al*., BMP restricts stemness of intestinal Lgr5^{+} stem cells by directly suppressing their signature genes. *Nat. Commun.* **8**, 13824 (2017).
31. X. Liao *et al*., Clinicopathological characterization of SMAD4-mutated intestinal adenocarcinomas: A case-control study. *PLoS One* **14**, e0212142 (2019).
32. J. Drost *et al*., Sequential cancer mutations in cultured human intestinal stem cells. *Nature* **521**, 43–47 (2015).
33. M. Matano *et al*., Modeling colorectal cancer using CRISPR-Cas9-mediated engineering of human intestinal organoids. *Nat. Med.* **21**, 256–262 (2015).
34. Z. Wiener *et al*., Oncogenic mutations in intestinal adenomas regulate Bim-mediated apoptosis induced by TGF-β. *Proc. Natl. Acad. Sci. U.S.A.* **111**, E2229–E2236 (2014).
35. F. Ramírez-Valle, S. Braunstein, J. Zavadil, S. C. Formenti, R. J. Schneider, eIF4GI links nutrient sensing by mTOR to cell proliferation and inhibition of autophagy. *J. Cell Biol.* **181**, 293–307 (2008).
36. J. Kong, P. Lasko, Translational control in cellular and developmental processes. *Nat. Rev. Genet.* **13**, 383–394 (2012).
37. J. D. Richter, N. Sonenberg, Regulation of cap-dependent translation by eIF4E inhibitory proteins. *Nature* **433**, 477–480 (2005).
38. S. Grüner *et al*., The structures of eIF4E-eIF4G complexes reveal an extended interface to regulate translation initiation. *Mol. Cell* **64**, 467–479 (2016).
39. R. Azar, A. Alard, C. Susini, C. Bousquet, S. Pyronnet, 4E-BP1 is a target of Smad4 essential for TGFbeta-mediated inhibition of cell proliferation. *EMBO J.* **28**, 3514–3522 (2009).
40. R. Colina *et al*., Translational control of the innate immune response through IRF-7. *Nature* **452**, 323–328 (2008).
41. A. Haghighat, N. Sonenberg, eIF4G dramatically enhances the binding of eIF4E to the mRNA 5′-cap structure. *J. Biol. Chem.* **272**, 21677–21680 (1997).
42. L. Jossé, J. Xie, C. G. Proud, C. M. Smales, mTORC1 signalling and eIF4E/4E-BP1 translation initiation factor stoichiometry influence recombinant protein productivity from GS-CHOK1 cells. *Biochem. J.* **473**, 4651–4664 (2016).
43. S. J. Baker *et al*., Chromosome 17 deletions and p53 gene mutations in colorectal carcinomas. *Science* **244**, 217–221 (1989).
44. E. Fessler *et al*., TGFβ signaling directs serrated adenomas to the mesenchymal colorectal cancer subtype. *EMBO Mol. Med.* **8**, 745–760 (2016).
45. M. van de Wetering *et al*., Prospective derivation of a living organoid biobank of colorectal cancer patients. *Cell* **161**, 933–945 (2015).
46. H. A. Crissman, J. A. Steinkamp, Rapid, simultaneous measurement of DNA, protein, and cell volume in single cells from large mammalian cell populations. *J. Cell Biol.* **59**, 766–771 (1973).
47. K. Haneke *et al*., CDK1 couples proliferation with protein synthesis. *J. Cell Biol.* **219**, e201906147 (2020).
48. M. Polymenis, R. Aramayo, Translate to divide: **C**ontrol of the cell cycle by protein synthesis. *Microb. Cell* **2**, 94–104 (2015).
49. C. C. Thoreen *et al*., A unifying model for mTORC1-mediated regulation of mRNA translation. *Nature* **485**, 109–113 (2012).
50. K. Düvel *et al*., Activation of a metabolic gene regulatory network downstream of mTOR complex 1. *Mol. Cell* **39**, 171–183 (2010).
51. Y. Martineau *et al*., Pancreatic tumours escape from translational control through 4E-BP1 loss. *Oncogene* **33**, 1367–1374 (2014).
52. T. Tian, X. Li, J. Zhang, mTOR signaling in cancer and mtor inhibitors in solid tumor targeting therapy. *Int. J. Mol. Sci.* **20**, E755 (2019).
53. K. E. Hung *et al*., Development of a mouse model for sporadic and metastatic colon tumors and its use in assessing drug treatment. *Proc. Natl. Acad. Sci. U.S.A.* **107**, 1565–1570 (2010).
54. P. Riemer *et al*., Oncogenic β-catenin and PIK3CA instruct network states and cancer phenotypes in intestinal organoids. *J. Cell Biol.* **216**, 1567–1577 (2017).
55. Q. Liu *et al*., Discovery of 1-(4-(4-propionylpiperazin-1-yl)-3-(trifluoromethyl)phenyl)-9-(quinolin-3-yl)benzo[h][1,6]naphthyridin-2(1H)-one as a highly potent, selective mammalian target of rapamycin (mTOR) inhibitor for the treatment of cancer. *J. Med. Chem.* **53**, 7146–7155 (2010).
56. A. Kentsis, I. Topisirovic, B. Culjkovic, L. Shao, K. L. B. Borden, Ribavirin suppresses eIF4E-mediated oncogenic transformation by physical mimicry of the 7-methyl guanosine mRNA cap. *Proc. Natl. Acad. Sci. U.S.A.* **101**, 18105–18110 (2004).
57. F. Pettersson *et al*., Ribavirin treatment effects on breast cancers overexpressing eIF4E, a biomarker with prognostic specificity for luminal B-type breast cancer. *Clin. Cancer Res.* **17**, 2874–2884 (2011).
58. K. P. Janssen *et al*., APC and oncogenic KRAS are synergistic in enhancing Wnt signaling in intestinal tumor formation and progression. *Gastroenterology* **131**, 1096–1109 (2006).
59. O. J. Sansom *et al*., Loss of Apc allows phenotypic manifestation of the transforming properties of an endogenous K-ras oncogene in vivo. *Proc. Natl. Acad. Sci. U.S.A.* **103**, 14122–14127 (2006).
60. K. Takaku *et al*., Intestinal tumorigenesis in compound mutant mice of both Dpc4 (Smad4) and Apc genes. *Cell* **92**, 645–656 (1998).
61. R. B. Halberg *et al*., Tumorigenesis in the multiple intestinal neoplasia mouse: Redundancy of negative regulators and specificity of modifiers. *Proc. Natl. Acad. Sci. U.S.A.* **97**, 3461–3466 (2000).
62. J. Wang, Q. Ye, Q.-B. She, New insights into 4E-BP1-regulated translation in cancer progression and metastasis. *Cancer Cell Microenviron.* **1**, e331 (2014).
63. A. Ohashi *et al*., Aneuploidy generates proteotoxic stress and DNA damage concurrently with p53-mediated post-mitotic apoptosis in SAC-impaired cells. *Nat. Commun.* **6**, 7668 (2015).
64. D. J. Murphy *et al*., Distinct thresholds govern Myc's biological output in vivo. *Cancer Cell* **14**, 447–457 (2008).
65. H. S. Hsu *et al*., The 4E-BP1/eIF4E ratio is a determinant for rapamycin response in esophageal cancer cells. *J. Thorac. Cardiovasc. Surg.* **149**, 378–385 (2015).
66. S. Grosso *et al*., Sensitivity of global translation to mTOR inhibition in REN cells depends on the equilibrium between eIF4E and 4E-BP1. *PLoS One* **6**, e29136 (2011).
67. A. Y. Choo, S. O. Yoon, S. G. Kim, P. P. Roux, J. Blenis, Rapamycin differentially inhibits S6Ks and 4E-BP1 to mediate cell-type-specific repression of mRNA translation. *Proc. Natl. Acad. Sci. U.S.A.* **105**, 17414–17419 (2008).
68. C. C. Thoreen *et al*., An ATP-competitive mammalian target of rapamycin inhibitor reveals rapamycin-resistant functions of mTORC1. *J. Biol. Chem.* **284**, 8023–8032 (2009).
69. A. Sriram, J. Bohlen, A. A. Teleman, Translation acrobatics: How cancer cells exploit alternate modes of translational initiation. *EMBO Rep.* **19**, e45947 (2018).
70. P. Alberici *et al*., Smad4 haploinsufficiency: A matter of dosage. *PathoGenetics* **1**, 2 (2008).
71. M. Morita *et al*., mTOR coordinates protein synthesis, mitochondrial activity and proliferation. *Cell Cycle* **14**, 473–480 (2015).
72. T. Sato *et al*., Single Lgr5 stem cells build crypt-villus structures in vitro without a mesenchymal niche. *Nature* **459**, 262–265 (2009).
73. J. Heijmans *et al*., ER stress causes rapid loss of intestinal epithelial stemness through activation of the unfolded protein response. *Cell Rep.* **3**, 1128–1139 (2013).
74. H. Shibata *et al*., Rapid colorectal adenoma formation initiated by conditional targeting of the Apc gene. *Science* **278**, 120–123 (1997).
75. E. L. Jackson *et al*., Analysis of lung tumor initiation and progression using conditional expression of oncogenic K-ras. *Genes Dev.* **15**, 3243–3248 (2001).
76. J. Jonkers *et al*., Synergistic tumor suppressor activity of BRCA2 and p53 in a conditional mouse model for breast cancer. *Nat. Genet.* **29**, 418–425 (2001).
77. B.-K. Koo *et al*., Controlled gene expression in primary Lgr5 organoid cultures. *Nat. Methods* **9**, 81–83 (2011).
78. J. F. Van Lidth de Jeude, J. L. M. Vermeulen, P. S. Montenegro-Miranda, G. R. Van den Brink, J. Heijmans, A protocol for lentiviral transduction and downstream analysis of intestinal organoids. *J. Vis. Exp.*, 52531 (2015).